Second Stage Actuation for Hard Disc Drives through MEMS Technology

Hans H. GATZEN[1], *Member, IEEE*, Paulo J. P. FREITAS[2], *Member, IEEE*, Ernst OBERMEIER[3], John ROBERTSON[4], *Member, IEEE*

[1]Leibniz Universitaet Hannover, Center for Production Technology, Institute for Microtechnology, Garbsen, Germany
[2]INESC MN, Microsystems & Nanotechnologies, Lisbon, Portugal
[3]Berlin University of Technology, Microsensor & Actuator Technology, Berlin, Germany
[4]University of Cambridge, Department of Engineering, Cambridge, United Kingdom

Taking advantage of Micro Electro-mechanical System (MEMS) technology, a Slider with an Integrated Microactuator (SLIM) for use in Hard Disc Drives (HDD) was devised. It allows both a lowering to the operating static flying height and a second stage actuation for ultra precision track following. By placing the read/write element on a small chiplet rather on the trailing edge of a slider, the design promises to be cost competitive. This paper provides an overview over the research results achieved so far. It discusses the fabrication technology applied for fabricating both the micromagnetics and micromechanics and presents experimental dynamic test results on SLIM devices which – although not yet flyable – do have fully functional microactuators.

***Index Terms*— Hard discs, Microactuators, Head, Microelectromechanical devices**

I. Introduction

FOR ACHIEVING an optimal read/write performance in Hard Disc Drives (HDD), a recording head has to reliably fly at a minimal height and has to be aligned perfectly with the data track to be written or read. To achieve a perfect track registration, the use of dual-stage actuators (DSA) has been suggested for quite a while [1]. In DSA servo systems, the conventional single-stage electromagnetic voice coil motor (VCM) acts as a coarse, low-speed, but large-stroke actuator, whereas a second microactuator acts as a fine, high-speed, but small-stroke positioning device. By combining them, the respective deficiencies of either one can be compensated. Therefore, a DSA system combines a large displacement with a high positioning accuracy and fast track seeking capabilities. There are three types of dual-stage system designs: moving suspension-type, moving slider-type, and moving head-type. Both moving suspension and moving slider-type solutions (the latter ones mostly Micro Electro-mechanical Systems (MEMS) based) were suggested. The moving suspension-type actuator is easier to fabricate compared with the other types of dual-stage systems. However, the servo bandwidth of this actuator type is limited to about 3 kHz due to the suspension resonance [2], [3], [4]. The second type of dual-stage actuators is the moving slider-type actuator, which is located between the suspension and the slider [5]. The advantage of this actuator is the co-location of the actuator and sensor, which provides a servo bandwidth of 5 kHz or even higher [6], [7]. A drawback of a moving slider-type actuator is that three additional wires are needed enhancing the wire number from four to seven. Furthermore, an additional assembly step is required since three instead of two parts have to be mounted. A PZT ceramic based type of a moving-slider microactuator for high track pitch HDDs was investigated by Hirano et al. [8]. Figure 1 shows an SEM image of the micro-actuator/slider/suspension assembly. A tracks-per-inch track density of more than 25,000 in a 3.5" HDD was demonstrated with this microactuator by the Hitachi San Jose Research Center. However, the total thickness of the suspension and actuator is large, and its assembly process is somewhat complicated.

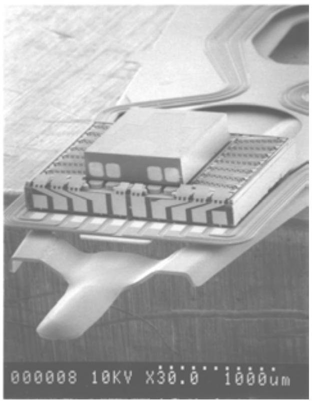

Fig. 1: SEM image of a PZT ceramic based moving slider-type actuator developed at the Hitachi San Jose Research Center.

The third type of dual-stage actuator is found between the drive and the read/write head [9]. It allows both flying height adjustment and track following.

The proposed innovative microactuator takes a fourth path: it places the second stage actuation between the slider body and the read/write element. One of its advantages is that the technology used for the fabrication of MEMS can be applied for its fabrication as well. Furthermore, the system features the dimensions of a standard pico size slider. This in combination with the potential for miniaturization and the enhancement of the resonant frequency creates a non-competitive system. In this respect, the trade-off between offset and resonant frequency is the determining parameter. The only disadvantage of the proposed system is that a cross crown is required on the bottom of the chiplet limiting the design of the read/write element.

Manuscript received August 21, 2009 (date on which paper was submitted for review). Corresponding author: Hans H. Gatzen (e-mail: gatzen@imt.uni-hannover.de).
Digital Object Identifier inserted by IEEE

II. CONCEPT

Analyzing DSA designs alternatives, the solution best suited for a cost neutral solution is the moving head- (i.e. moving read/write element) type. It bears the potential for compensating the costs for the second stage actuator by reducing the fabrication costs of the read/write element. The approach suggested is as follows [10]: instead of placing the read/write element at the trailing edge of the slider itself, it will be located on a chiplet only the third the size of the slider (the chiplet will also be actuated). This way, two thirds of the slider fabrication costs are freed up, with one third of the costs earmarked for a MEMS technology type Slider with an Integrated Microactuator (SLIM) and the other third reserved for system integration. For the device suggested, an electromagnetic microactuator activates a mounting block to which a chiplet is attached. The read/write element is located at the chiplet's trailing edge. The actuator allows two motions: a vertical displacement for lowering the read/write element to the (quasi-static) flying height; this allows to lowering the chiplet only in case of a Head Select. It further enables a (very slight) rotation executing a lateral displacement for track following.

III. DESIGN AND TECHNOLOGY

The SLIM follows the basic dimensions of a pico-form factor slider (1,240 µm x 990 µm x 300 µm). For its fabrication, MEMS technology is applied, using a two-wafer approach. The bottom wafer contains the micromagnetics, consisting of a pair of variable reluctance (VR) microactuators. The actuator mechanics reside in the top wafer, they consist of a slider body and a mounting platform suspended by a pair of leaf springs. The mounting platform carries the chiplet containing the read/write element. A desired lateral displacement of 625 nm (corresponding to ±5 tracks at

a)

b)

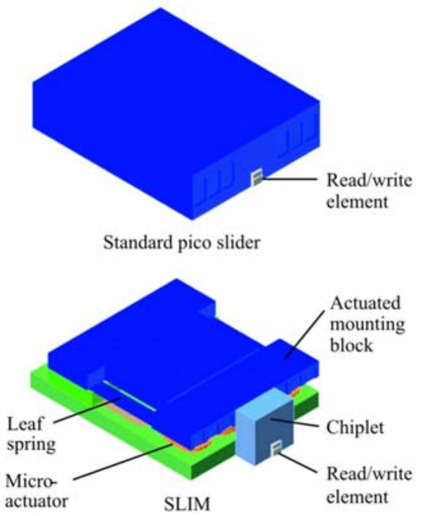

Fig. 2: Comparison between sliders: a) standard pico slider; b) Slider with an Integrated Microactuator (SLIM).

200 ktpi) requires a rotation of 0.18° [11]. The design goal set by the industry at the beginning of the program was a track following frequency of 3 kHz. However by increasing the leaf spring thickness, the resonance frequency may be increased appropriately, but will result in a reduced lateral travel. This way, an optimum between resonance frequency and secondary actuation capability may be chosen. Fig. 2 compares a standard pico slider and SLIM.

While the SLIM allows to lowering the read/write element to the desired static flying height, this approach is not expected to compete with a thermal flying height control (TFC) for a dynamical flying height adjustment. Therefore, an implementation of TFC within the SLIM has been intended since the start of the program. This is accomplished by providing two extra control lines for a heating resistor.

A. *Actuator Micromagnetics*

For fabricating the SLIM micromagnetics, high aspect ratio micro structure technology (HARMST) is applied. An electroplating process created the NiFe45/55 flux guide, as well as dual layer Cu spiral coils. Fig. 3 shows a schematic representation of the SLIM micromagnetics.

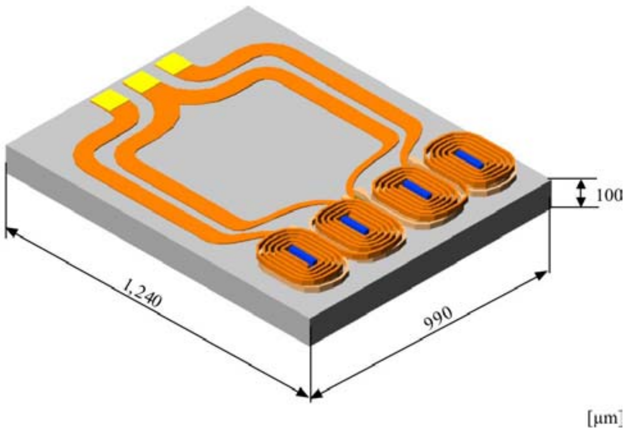

Fig. 3: SLIM micromagnetics.

The actuator magnetics consists of a pair of variable reluctance (VR) microactuators. The fabrication is carried out on a 525 µm thick Si wafer, which ultimately has to be thinned to the desired device height of 100 µm. The

a) b)

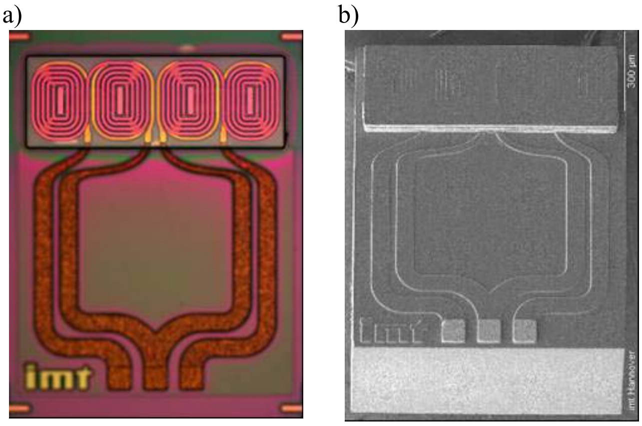

Fig. 4: Fabricated SLIM micromagnetics: a) optical micrograph; b) SEM micrograph.

microactuator itself consists of double-layer Cu spiral microcoils with a C-shaped soft magnetic core made of NiFe45/55. For the fabrication of the microactuators in thin-film technology, a combination of photolithography and electroplating was chosen. This is accomplished by creating micro molds made of positive photoresist used for the electro-deposition of the NiFe45/55 and Cu structures, respectively. The horizontal insulation layer between the two coil layers as well as between the coils and the core are made of Si_3N_4, which is deposited by a Plasma Enhanced Chemical Vapor Deposition (PECVD) process. For the lateral embedding, the photosensitive epoxy SU-8™ is used. Several Chemical-mechanical Polishing (CMP) steps are required during the fabrication to provide an even surface before the next thin-film is deposited and patterned. Finally, dual-stage microactuators with NiFe45/55 C-shaped cores and double-layer Cu spiral coils are available. Fig. 4 shows micrographs of a completed micromagnetics device. The functionality device on a micromagnetics level was verified by Scanning Hall Probe Microscopy Measurements [12], [13].

B. *Actuator Micromechanics*

For the fabrication of the actuator mechanics device, SOI-wafers with two device layers were employed. The SOI-substrate has an overall thickness of 300 µm and the two device layers have a total thickness of 100 µm. One ultimately forms the micromechanics body and the other the leaf springs. The thickness of the device layer on the top defines the leaf spring thickness. The two buried oxide layers with a thickness of each of 0.3 µm serve as etch stop layers during the processing. Fig. 5 shows the main fabrication steps. They are electroplating of flux guide (Fig. 5a)) structures; b) etching of cavities for sidewall contacts (Fig. 5b)); metallization and realization of bond pads (Fig. 5c)); patterning of leaf springs (Fig. 5d)); e) release of leaf springs from the top (Fig. 5e)) [11].

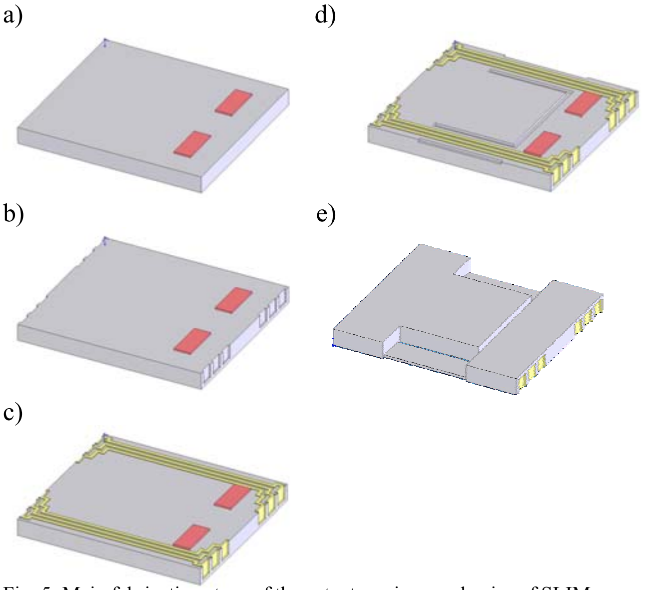

Fig. 5: Main fabrication steps of the actuator micromechanics of SLIM.

C. *SLIM Stacking*

After completing the fabrication processes for the magnetics as well as the mechanics, both wafers are cut into double rowbars with two rows of ten SLIM devices each facing each other. At this level, the SLIM components are stacked. Each double rowbar consists of 20 SLIM devices, which are arranged in a 10x2 array. Fig. 6 illustrates an exploded view of the main steps of the assembling process. Fig. 7 shows the double rowbar on a one Euro Cent coin.

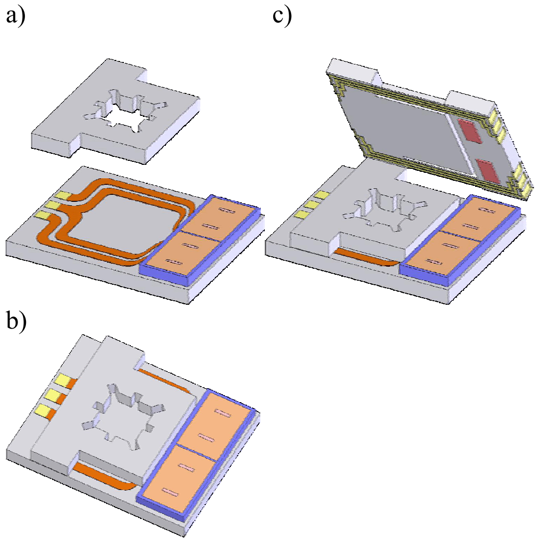

Fig. 6: SLIM assembly (demonstrated on a single SLIM device); a) alignment of spacer to actuator magnetics; b) adhesive bonding of spacer to actuator magnetics; c) alignment and adhesive bonding of actuator mechanics to spacer and actuator magnetics.

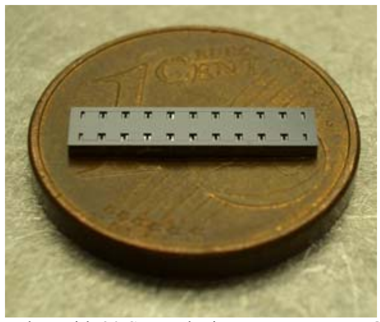

Fig. 7: Double rowbar with 20 SLIM devices on a one Euro Cent coin.

After the stacking is completed, the double rowbar has to be thinned to a thickness of 300 µm. The reason is that the micromagnetics fabrication was executed on a 525 µm thick wafer. The height reduction was performed by a thinning by dicing process, followed by a nanogrinding and CMP process [14]. Thinning by dicing is a process where the wafer first is grooved in a dicing process. In a second step, the land areas created by the grooving are removed in a second grinding run. Fig. 8 shows an unthinned and a thinned double rowbar.

D. *Slider ABS*

The next step after completing the slider stacking process was creating the air bearing surface (ABS) at the bottom of the double rowbars. During the first runs, the test devices were fabricated without an ABS, yielding devices with functional microactuators, but not capable of flying. Nevertheless, a process for future creating the ABS on the double rowbars was developed.

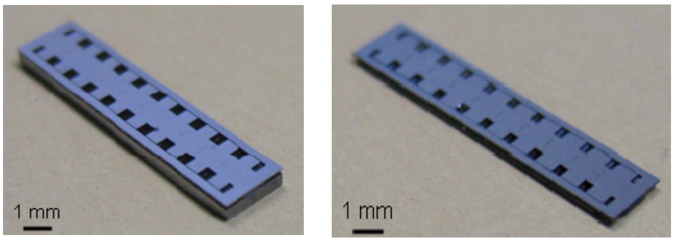

Fig. 8: Unthinned and thinned double rowbar.

The ABS pattern for the slider was designed and simulated by Prof. Talke, University of California, San Diego (UCSD). All simulation results were obtained for a rotational disc speed of 7,200 rpm. The optimized sub-ambient pressure ABS design is shown in Fig. 9.

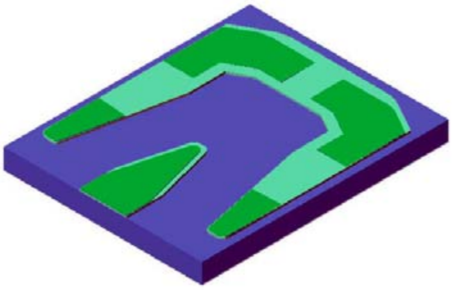

Fig. 9: Final sub-ambient pressure slider ABS design for SLIM.

The ABS structure consists of two different levels. The first (lower) level has a depth of 1 µm, the second level a depth of 260 nm. As fabrication technology, ion beam etching (IBE) was applied. For the preliminary tests, a fabrication on wafer level was carried out. A variation of photoresists was tested for finding out the most suitable resist. The most critical fabrication step is the etching of the first level of 1 µm depth into the Si since the photoresist must withstand the long etching process. Fig. 10 shows a Si dummy double rowbar after the completion of the first ABS etch step.

a) b)

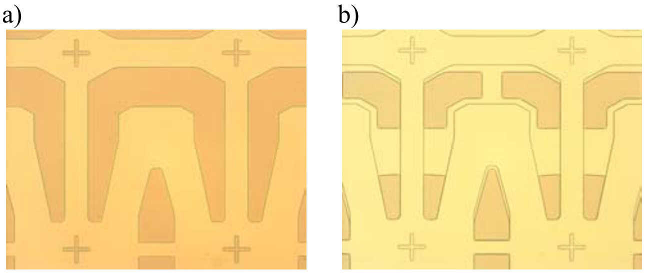

Fig.10: ABS-design on wafer level; a) first level finished, b) completed design.

The results from technological tests on wafer level were used for the fabrication of the sub-ambient pressure design on double rowbar level. Since a process to fabricate the ABS on single double rowbars was required, a handling tool to execute the photolithography process was devised. It consists of a 300 µm thick Si wafer bonded to a glass carrier wafer using Aquabond^{TM}. The Si wafer contained a central opening with the dimensions of a diced double rowbar. For a simple removal of the double rowbar, the glass wafer is equipped with a hole in the area of the opening for the double rowbar. First tests showed that a central arrangement of the opening was not practical since it created bubbles appearing at the edges of the double rowbar during resist spin-on. Therefore, two alternative versions of a handling tool with a pair of quasi radial and quasi tangential openings were developed (Fig. 11a) and 11b)). It was found out that there is no significant difference between both versions, each one is practical.

a)

b)

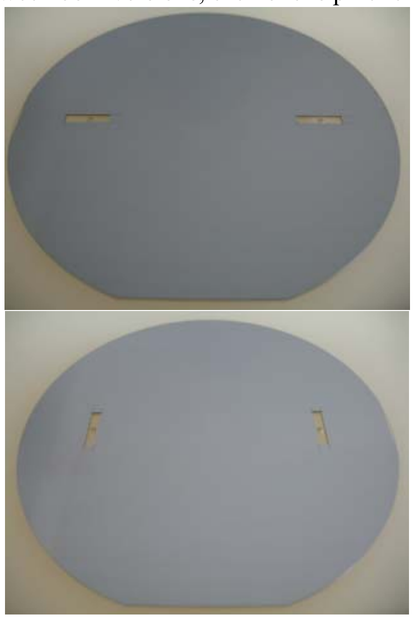

Fig. 11: Optimized handling tool with two openings; a) openings quasi-radial, b) openings quasi-tangential

The initial process tests were conducted with Si dummy double rowbars. Fig. 12 depicts such a part with the first level of the ABS-design as an optical micrograph.

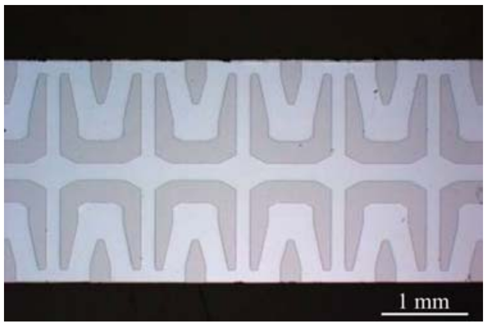

Fig. 12: Optical micrograph of the first ABS etch step on a Si double rowbar dummy.

For an evaluation of the ABS design, Si dummy sliders, which featured both the ABS and a DLC coat (see below) were mounted on a flexure, such creating a flyable dummy head assembly (Fig. 13). Flying height tests were conducted at AheadTek Inc., San Jose, CA. In these tests, a stable flight at approximately 10 nm up to 7,200 rpm could be achieved, which verified the functionality of the UCSD ABS design for SLIM.

E. DLC Coat

Diamond-like carbon (DLC) is widely used for corrosion and wear protection in hard disc drives because it is amorphous, hard, smooth, pin-hole free down to thickness of ~1 nm, and with a low friction coefficient [15], [16]. It can be produced by a variety of plasma deposition techniques. Here we use a hydrogen-free type of DLC called "tetrahedral amorphous carbon" or ta-C, deposited by filtered cathodic vacuum arc (FCVA) [17]. The DLC films are grown at a base pressure of 10^{-7} mbar, ion energy 100 V and growth rate of 6 Å/s. The substrates were subjected to cleaning in acetone and DI water. DLC was deposited to a thickness of 30 nm on the slider surfaces. Fig. 14 depicts a DLC coated Si dummy test slider with ABS.

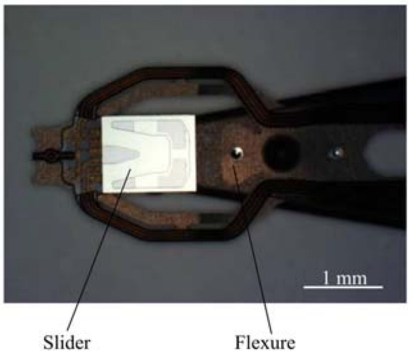

Fig. 13: SLIM head assembly with Si dummy slider with the ABS and a DLC coating.

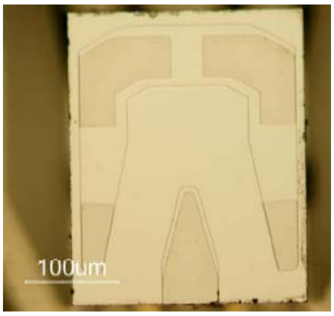

Fig. 14: Optical micrograph of carbon-coated slider with ABS before tribological testing.

The tribological properties of the surfaces were tested on a rotating wear tester, for up to 1,200 test cycles (26 hours duration). Fig. 15 shows a friction sweep plot.

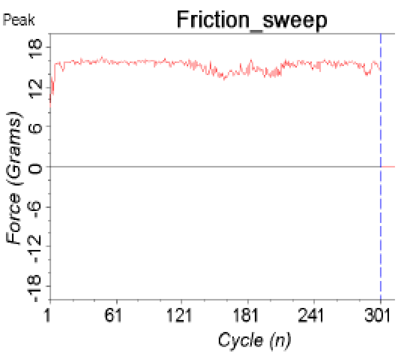

Fig. 15: DLC test friction sweep plot.

F. Chiplet Mounting and Slider Dicing

In a first step, the double rowbars were sliced into single rowbars. This process also opened up the leading edge contact pads, allowing to doing a resistance test at the actuator coils to verify which systems promise to be functional.

Next, the chiplets were mounted to the mounting platform. Ultimately, a chiplet is intended to carry the read/write element. For mounting the chiplet, a specific assembly tool was developed, which allows to registering the chiplet at the appropriate height (i.e. flush with the slider ABS) and at the desired location (exactly at the slider's center) on the mounting platform. The bottom of the fixture is a porous ceramic vacuum chuck, which holds down the chiplet by suction, but still allows to adjusting its position by shifting it. A micrometer screw registers the rowbar appropriately to a reference tool. The chiplet is manipulated with a vacuum needle. First, a drop of adhesive (cyanoacrylate) is administered. Next, the chiplet is placed on the vacuum chuck and slid against the mounting bar using a slide. Finally, it is pushed against the reference surface by means of the vacuum needle and held until the adhesive is cured.

After the chiplet was mounted, a slider dicing process is conducted. This process is very delicate, since it not only separates the slider, but also releases the 5 µm thick leaf springs suspending the mounting platform. The process isexecuted with the rowbar bonded to a thermal release tape.

One of the key requirements for the SLIM design to function is that the chiplet is actually capable of a slight rotation. As a result, the chiplet has to receive a cross crown. This cross crown will be created by a kiss-lap process, either on a slider level or on a head assembly level. ABS simulations conducted by Prof. Talke, UCSD, showed, that such a chiplet with cross crown should have no air bearing capability, which is advantageous for the desired application. For the non-flying tests, no such cross crown was required.

G. Head Assembly

For gaining a complete head (slider flexure) assembly, the slider has to be mounted on a flexure and electrically connected. On existing heads, the contacts are on the trailing edge of the slider. For SLIM, this contact area is not feasible since the trailing edge of the slider features the very delicate, actuated mounting bar with the chiplet. Therefore, for SLIM the electrical connections are at the SLIM's leading edge.

For SLIM, a commercial flexure recommended by Seagate Technology and supplied by Magnecomp was used. First, the wires were bonded to the three contact pads leading to SLIM's two electromagnets. Next, these three wires were spliced into the existing flex cables. Then, the slider was bonded to the flexure. The bonding tool used for this process was developed and built by AheadTek. Fig. 16 presents a comparison between a classic HDD head (Seagate Momentus 5.400.3) and a non-flyable SLIM head assembly.

III. Experimental Investigations

A. Control Box and Test Fixture

The actuators are powered by a current provided by an actuator control box. It has been designed as a high resolution power supply for low resistance range. The voltage is written by a microcontroller to two independent 16 bits DAC. The signal is then fed to low-noise power amplifiers and then to the SLIM coils. Two calibrated resistors placed on the current path of the two channels are used to measure the current actually passing through the coils in order to provide a feedback used to regulate the current around its setpoint. The power supply can provide 200 mA at 15 Ω, which allow the operation of the SLIM actuator through the resistance felt along the flexure and through the wire-bonding. Fig. 17 shows the set-up of the SLIM control system.

a)

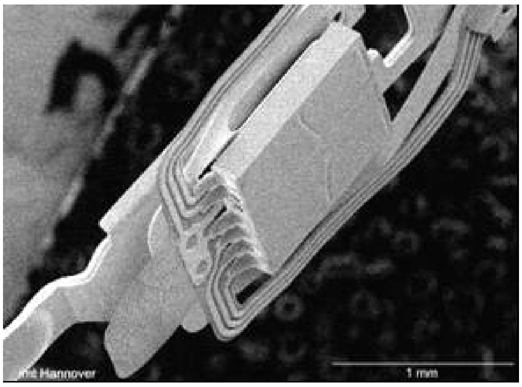

b)

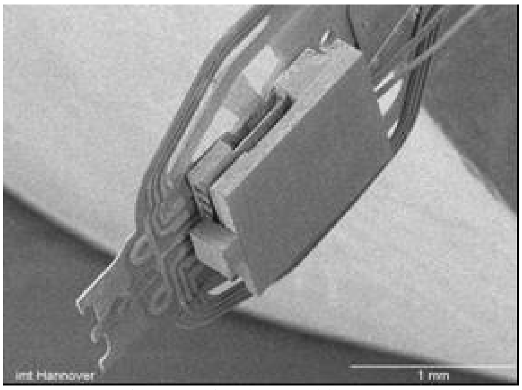

Fig. 16: Comparison between head assemblies: a) typical HDD head; b) SLIM head assembly (without ABS).

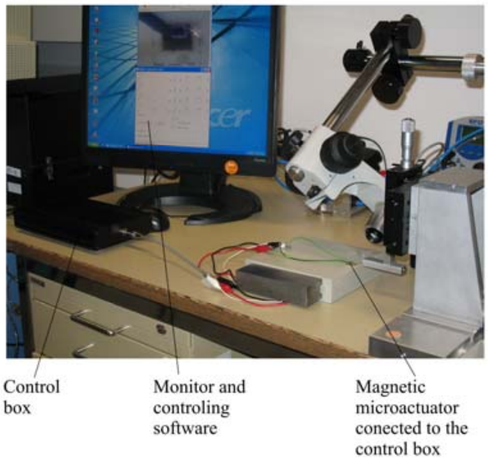

Fig. 17: SLIM Control system.

The microcontroller is programmed update the current at a frequency up to 15 kHz. However the amplification chain architecture provides a full signal bandwidth of 50 kHz and could operate at small signals (as required for drive regulation) at up to 170 kHz. The limitation to the operating frequency is given by the slew rate of 9 mA/µs. While the resolution is 3 µA, the frequency noise level for frequencies higher than 100 Hz is less than 2 nA/√Hz, allowing a very high signal-to-noise ratio. The characteristics of the SLIM control box noise are shown in Fig. 18.

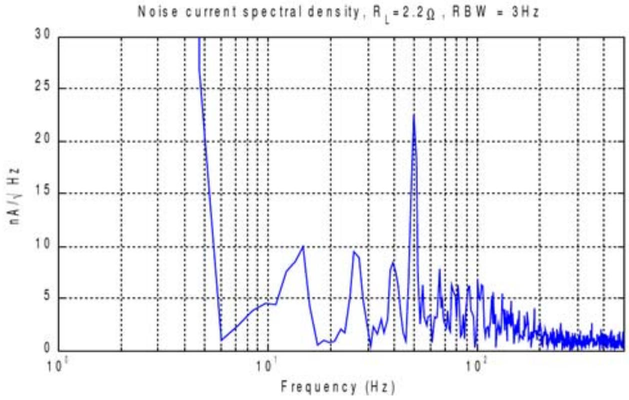

Fig. 18: SLIM control box noise characterization in the range of 5 Hz to 500 Hz. A peak at 50 Hz is visible. Noise at higher frequency is lower than 2 nA/√Hz.

The microcontroller allows the implementation of a command and/or regulation algorithms for practical operation of the device. It allows to commanding independently the two channels and provides functions for rotation and height control of the actuator. The actuation system, although autonomous for its operation procedures, can send data and receive asynchronous control from a computer through USB connection.

For executing actuation tests in the non-flying state, a test fixture was designed and fabricated (Fig. 19). It allows to mounting the SLIM head assembly in a way that mounting bar and chiplet can be actuated freely.

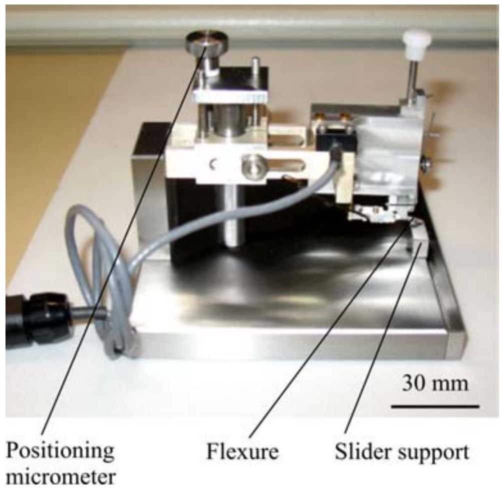

Fig. 19: SLIM actuation test fuxture for non-flyable heads.

B. Magnetic Force Verification

To verify the magnetic force curves of the microactuator, a comparison between the simulation results and the actual device behavior was conducted. To do so, a force sensor with a magnetic material serving as flux closure was devised. Fig. 20 shows the results. For air gaps greater than 15 µm, a good correlation between the simulation and the measurement results was found. The deviations at lower gap lengths are more a sign for the measurement difficulty for small gap lengths rather than a proof for an actual discrepancy.

Furthermore, an extensive operating range optimization was conducted. It aimed at finding the optimal air gap between the microactuator's active part and the flux guides on the mounting bar [18].

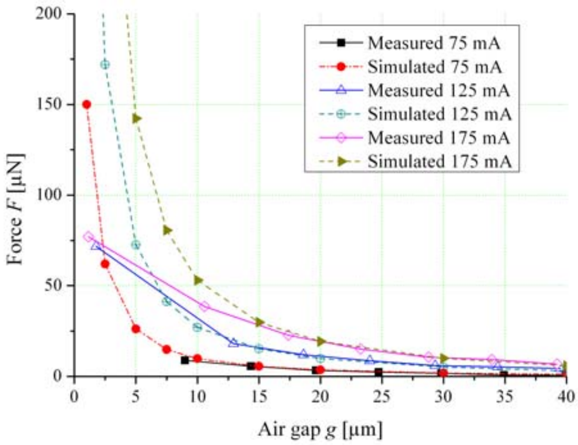

Fig. 20: Comparison of simulated and measured magnetic force as a function of the air gap and excitation.

C. Laser Doppler Vibrometry (LDV) Measurements

One of the most important information required regarding SLIM is its resonance frequency behavior. Based on the design, the first resonance mode (vertical translatory vibration) is responsible for the quasi-static flying height adjustment, while the second resonance mode (rotational vibration) describes the track following characteristics. To analyze the behavior, resonance frequency FEM simulations were compared to actual measurements using Laser Doppler Vibrometer (LDV) measurements. Fig. 21 shows the LDV system by Polytec.

Fig. 21: LDV test system.

Fig. 22 depicts the measurement spots. Beam 1 was used for deflection measurements analyzing the translatory displacement of the mounting bar. The location of beam 2 allowed to picking up the rotatory motion.

To influence the resonance behavior, there was a variation of the geometry of the leaf springs suspending the mounting platform. While all leaf springs had the same length of 300 µm, two width (100 µm and 150 µm) and two thicknesses (5 µm and 15 µm) were built.

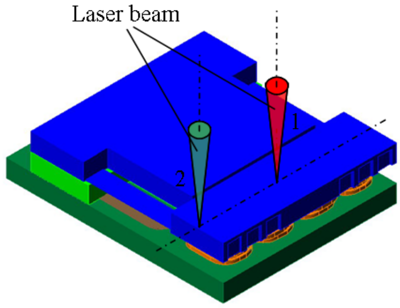

Fig. 22: LDV measurement points.

Fig. 23 shows the results of the resonance frequency measurement using the LDV measurements system. The measuring system allows to determining the measuring area of interest and shows as a result the oscillating frequency and form of the oscillation. Fig. 23 present vibrational modes; Fig. 23a) depicts the translational oscillation (first harmonic) while Fig. 23b) the rotational form of the oscillation (second harmonic).

a)

b)

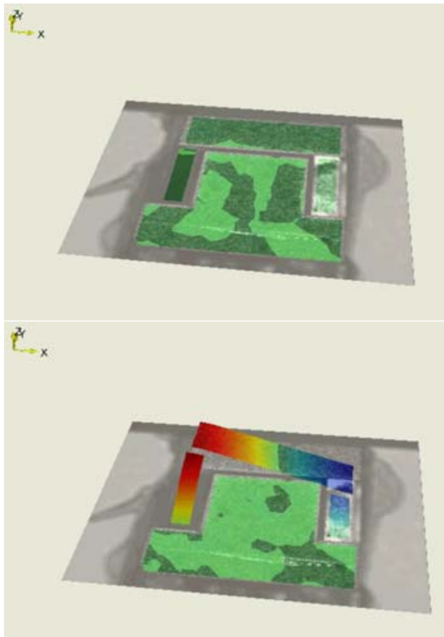

Fig. 23: Vibrational mode measurement results: a) First resonance mode (translational = flying height adjust); b) Second resonance mode (vibrational = track following).

Table I presents a comparison between simulation and measurement results. In both cases, the mounting platform behavior without chiplet was analyzed. The result confirms previous investigations which concluded that leaf springs with a width of 150 µm and a thickness of 5 µm represented a good compromise between displacement and resonant frequencies. In that case, the resonance frequency for track following mode (second harmonic) is in the range of 4.5 to 6 kHz. It also shows that the resonance frequency can be substantially increased, if a stiffer leaf spring is chosen. However, this solution requires a compromise regarding displacement.

Table I
Natural Resonance Frequencies

Leaf spring geometry: L x W x T [µm]	First harmonic [kHz]		Second harmonic [kHz]	
	Simul'n	LDV	Simul'n	LDV
500 x 100 x 5	0.88	0.86	5.3	2.75
500 x 150 x 5	1.07	1.46	6.14	4.76
500 x 100 x 15	4.54	6.15	25.4	-
500 x 150 x 15	5.55	-	29.2	-

IV. SLIM Pros and Cons

The main challenge of SLIM is the fact that the chiplet carrying the read/write element has to be contoured with a cross crown. This prerequisite is a consequence of the actuation scheme requiring a rotation (also very slight) of the chiplet to accomplish a lateral displacement of the transducer. For that reason, the read/write element may not feature any pieces of greater width requiring a close contact to the disc. This drawback is compensated by many advantages. Due to the fact, that the read/write transducer is located on a chiplet, the fabrication processes for the microactuator and the read/write element are clearly separated. Furthermore, this approach is very cost competitive. The advantage is twofold: (1) the read/write element fabrication costs are greatly reduced do to the small chiplet size and (2) the microactuator fabrication costs will dramatically decrease with growing fabrication numbers due to the automation potential typical for MEMS device fabrication. Last but not least, the actuation principle is magnetic, a technology the magnetic recording community is very familiar with.

V. Conclusion and Outlook

The work conducted with the Slider with an Integrated Microactuator demonstrates that an integrated MEMS based approach for a second stage actuator results in a cost competitive solution. Tests conducted so far proved the feasibility of the concept. Future work will extend the experimental investigations to SLIM devices actually flying.

Acknowledgment

This work was sponsored in part by the European Commission within the Framework 6 Information Society Technologies Programme's Specific Target Research Project (STREP) PARMA (Performance Advances in Recording through Micro Actuation). Furthermore, the authors are indebted to Seagate Technology, Bloomington, MN, for supporting the program with parts, test equipment and advice, F. Talke, UC San Diego for conducting the ABS simulations, and T. Higgins, AheadTek, San Jose, CA for enabling flying height tests.

References

[1] L.-S. Fan, H. H. Ottesen, T. C. Reiley, and R. W. Wood, "Magnetic recording head positioning at very high track densities using a microactuator-based, two-stage servo system," *IEEE Trans. Ind. Electron.*, **42** (3), 222–233, 1995.

[2] I. Takahiro, K. Masaki, I. Yukinori, O. Takeshi, K. Ryosuke, and K. Takao, "MEMS-based integrated head/actuator/slider for hard disk drives," IEEE/ASME Trans. Mechatron **3** (3), 166–174, 1998.

[3] Z. He, G. Guo, L. Feng, W.E. Wong and H.T. Loh, „Microactuation mechanism with piezoelectric element for magnetic recording head positioning for spin stand," *Journal of Mech. Engineering Science*, **220**, No. 9, pp. 1455-1461, 2006.

[4] Z.W. Zhong, and J. Sun, "A suspension integrated with a piezoelectric microactuator for dual stage actuation," *The International Journal of Advanced Manufacturing Technology*, **24**, No. 9-10, pp. 686, 2004.

[5] Y. Jing and J. B. Luo, "Processing and thickness effects on the microstructure and electrical properties of sol-gel deposited Pb(Zr, Ti)O films," Sens. Actuators A: Phys. **121**, 103–112, 2005.

[6] T. Imamura, T. Koshikawa, and M. Katayama, "Transverse mode electrostatic microactuator for MEMS-based HDD slider," in Proc. IEEE MEMS Workshop, 216–221, 1996.

[7] T. Hirano; M. White; Henry Yang; K. Scott; S. Pattanaik; S. Arya and Fu-Ying Huang, "A moving-slider MEMS actuator for high-bandwidth HDD tracking," Magnetics, *IEEE Trans. on Magn*., **40**, No. 4 (2), pp. 3171-3173, 2004.

[8] T. Hirano, H. Yang, "A hard-disk drive tracking servo microactuator driven by PZT with stroke amplification mechanism", Transducers, International Conference on Solid-State Sensors and Actuators **13**, 409-412, 2005.

[9] S. Nakamura, H. Numasato, K. Sato, M. Kobayashi, and I. Naniwa, "A push-pull multi-layered piggyback PZT actuator," Microsyst. Technol. **8**, 149–154, 2002.

[10] H.H. Gatzen, "Schreib-/Lesekopf mit integriertem Mikroaktor (Read-Write Head with Intergrated Microactuator)," German Patent 10260009, (2004) / U.S. Patent Application 10/540,119

[11] H.H. Gatzen, P.J. Freitas, E. Obermeier, and J. Robertson, "A Slider with an Integrated Microactuator (SLIM) for Second Stage Actuation in Hard Disc Drives," *IEEE Trans. Magn.*, **44** (11), 3726-3729, 2008.

[12] D. Dinulovic, H. Saalfeld, Z. Celinski, S. Field, H.H. Gatzen: Integrated Electromagnetic Second Stage Microactuator for a Hard Disk Recording Head. *IEEE Trans. on Magn*. **44**, No. 11, pp. 3730-3733, 2008.

[13] Dinulovic, H. Saalfeld, Z. Celinski, S. Field, H.H. Gatzen: Evaluation of an Electro-magnetic Micro Actuator Using Scanning Hall Probe Microscopy Measurements. MMM, 53rd Conf. on Magnetics and Magn. Materials, Austin, TX, USA, Abstracts, FE-10, 2008, Journal of Applied Physics **105**, 07F119-1, 2009.

[14] S. Cvetkovic, H. Saalfeld, H.H. Gatzen: Dicing Process for the Device Separation of a Slider with an Integrated Microactuator (SLIM). Proc. ASPE 23rd Ann. Meet. 2008 and 12th ICPE, Portland, OR, USA, pp. 380-383, 2008.

[15] J. Robertson, 'Diamond-like Amorphous Carbon', Mat Sci Eng R **37** 129-281, 2002.

[16] J. Robertson, "Requirements of ultrathin carbon coatings for magnetic storage technology", Trib Int **36**, 405-415, 2003.

[17] M.C. Polo, J.L. Andujar, A. Hart, J. Robertson, W.I. Milne, "Preparation of ta-C films by filtered cathodic vacuum arc", Diamond Related Mats **9**, 663, 2000.

[18] D. Dinulovic, F. Pape, H. Saalfeld, W. Kurniawan, E. Obermeier, H.H. Gatzen: Operating Range Optimization of a MEMS Type Slider with an Integrated Microactuator (SLIM) for Second Stage Actuation in Hard Disc Drives. *IEEE Trans. on Magn*. **45**, No. 10, pp. 3769-3772, 2009.